IMPLEMENTATION OF COMPUTER PROCEDURES AND STRESS-STRAIN LAWS IN GEOTECHNICAL ENGINEERING

Edited by

C.S. Desai
and
S.K. Saxena

Volume II

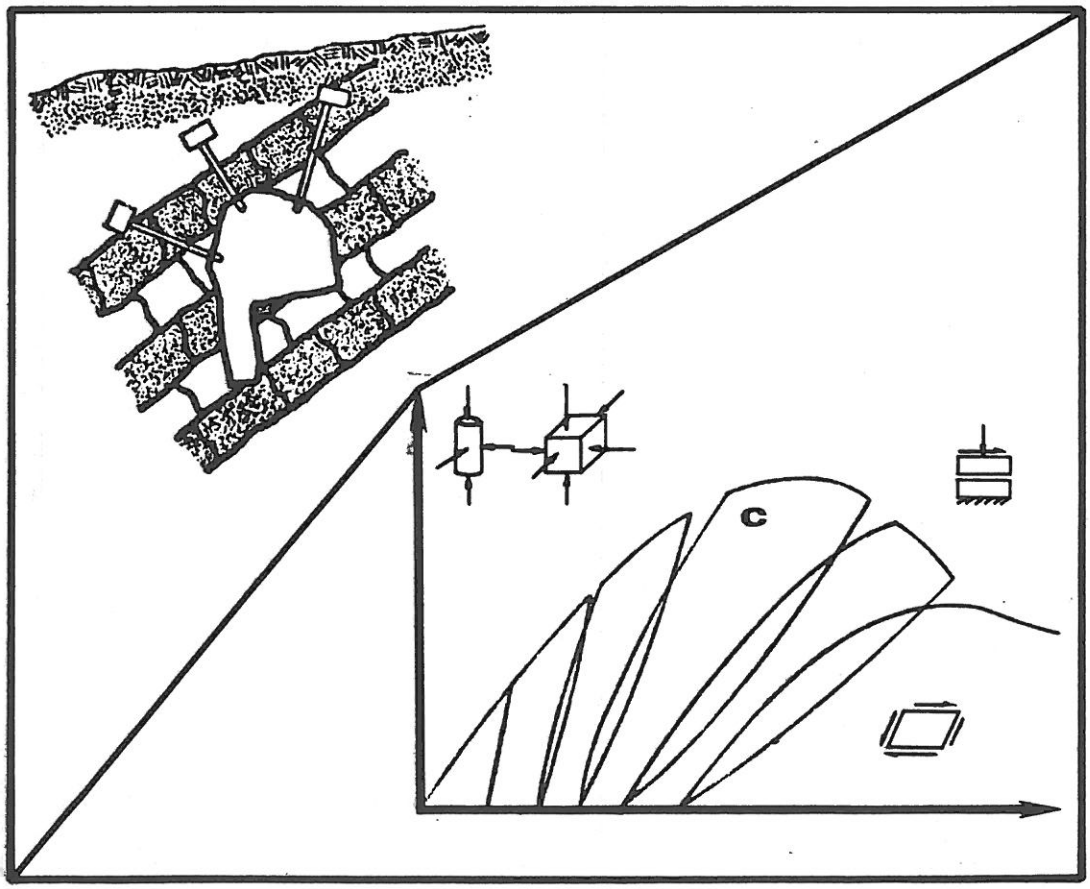

COMPUTATION OF STRAIN SOFTENING BEHAVIOUR

D.V. Griffiths
Lecturer, Simon Engineering Laboratories, University of Manchester, England

SUMMARY

Using simple numerical models, the influence of various stress/strain paths, both pre- and post-peak is examined with reference to ultimate earth pressure conditions. Both cohesive and frictional soils which strain soften are considered, and progressive failure is reproduced numerically leading to ultimate loads that are dependent on the degree of post-peak brittleness.

Although all calculations assume the soil to remain a continuum, the finite element solutions are observed to give a good indication of the failure surfaces along which large relative movements occur.

INTRODUCTION

When the stress/strain behaviour of a soil is referred to, it must be asked, "What stress, and what strain?" In a triaxial test, the stress/strain behaviour is conveniently expressed in terms of a deviator stress and an axial strain. In continuum two- or three-dimensional problems, triaxial stress states practically never occur, so a more general stress/strain relation must be used that takes account of the fact that all the shear and normal components of stress and strain may now be non-zero.

Undrained clay behaviour is a convenient material to work with because in theory, its strength and stress/strain path to failure in a triaxial test is independent of confining pressure. Deviatoric invariants of stress and strain are suggested for such a material where in plane strain:

$$\bar{\sigma} = \frac{1}{\sqrt{2}} \left[(\sigma_x - \sigma_y)^2 + (\sigma_y - \sigma_z)^2 + (\sigma_z - \sigma_x)^2 + 6\tau_{xy}^2 \right]^{\frac{1}{2}} \quad (1)$$

$$d\bar{\varepsilon} = \frac{\sqrt{2}}{3} \left[(d\varepsilon_x - d\varepsilon_y)^2 + (d\varepsilon_y - d\varepsilon_z)^2 + (d\varepsilon_z - d\varepsilon_x)^2 + \frac{3d\gamma_{xy}^2}{2} \right]^{\frac{1}{2}} \quad (2)$$

These invariants have the advantage that under triaxial conditions, $\bar{\sigma}$ reduces to the familiar deviator stress. Although these are the deviatoric stress and

strain invariants used in the present work, some workers prefer to use t and $\bar{\gamma}$ where

$$t = \sqrt{\frac{2}{3}}\ \bar{\sigma} \tag{3}$$

and

$$d\bar{\gamma} = \sqrt{\frac{3}{2}}\ d\bar{\varepsilon} \tag{4}$$

as these represent actual lengths in principal stress or strain space.

Whatever invariants are eventually chosen, they must be compatible from an energy viewpoint. If σ_m and $d\bar{v}$ are the volumetric invariants of stress and strain where

$$\sigma_m = (\sigma_x + \sigma_y + \sigma_z)/3 \tag{5}$$

$$d\bar{v} = (d\varepsilon_x + d\varepsilon_y + d\varepsilon_z) \tag{6}$$

then the total energy supplied to an element of material is given by the product of these invariants thus[1]

$$dE = \bar{\sigma}\ d\bar{\varepsilon} + \sigma_m\ d\bar{v} \tag{7}$$

It may also be noted that under elastic conditions

$$\frac{\bar{\sigma}}{\bar{\varepsilon}} = 3G\ . \tag{8}$$

Fig.1 gives three invariant stress/strain paths that are proposed for implementation in a continuum problem. Curve A represents familiar elastic-

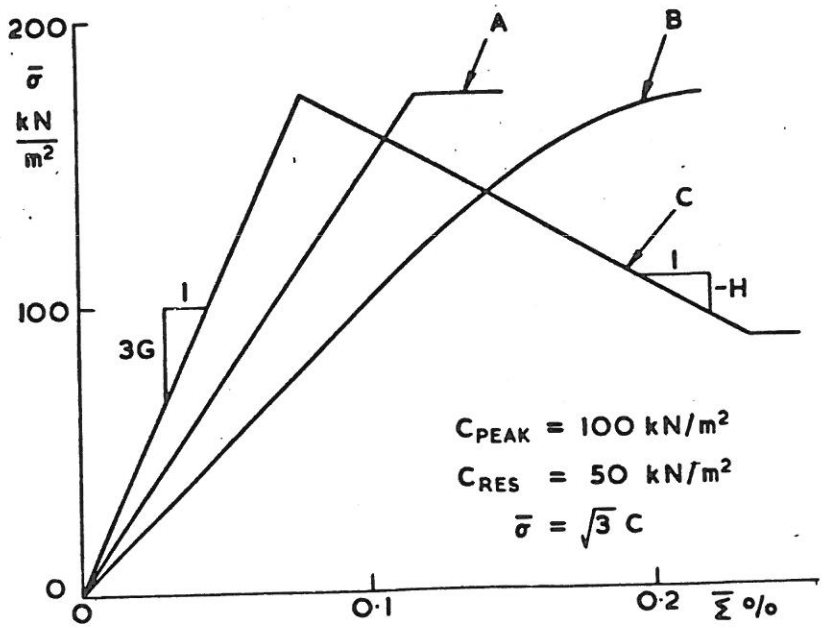

Fig.1 Cohesive Stress/Strain Laws

perfectly plastic material behaviour, curve B reaches its peak strength in a smoother fashion, exhibiting both elastic and plastic strains throughout the stress path, and curve C shows a strain-softening behaviour following an initial elastic phase. Curve B for example, could be fitted to typical triaxial stress/strain curves obtained with a normally consolidated clay. Curve C approximates the behaviour of some clays and especially sensitive clays where shear strains result in changes in structure of the clay and a corresponding reduction in strength. This decrease in strength is thought to be due to the reorientation of plate-like clay particles parallel to the failure surface. The difference between peak and residual strength in silty clays is usually small, but increases with clay content. The difference also tends to increase with increasing overconsolidation ratio.

Dense sands at moderately low confining pressure also exhibit strain-softening, but due to a different mechanism. The post-peak reduction in strength in this case is due to the interlocking component of strength in the sand having been overcome.

The significance of the strain-softening portion of a stress/strain curve may not be important if small shear displacements are anticipated in a given field problem. If this is not the case however, it would be unconservative to rely on peak strengths in design. The phenomenon of progressive failure was discussed by Rowe and Peaker[2] in the passive wall problem. They found that the maximum resistance of a passive wall corresponded to a friction angle that lay between the peak and residual values.

The stress/strain models proposed for frictional soil given in Fig.2 include an elastic, perfectly plastic material (Curve A) and a softening material (Curve B) that employs a step reduction in strength from peak to residual. These curves are written in terms of stress ratio and axial strain because unlike the clay, no unique $\bar{\sigma} - \bar{\varepsilon}$ relationship is applicable.

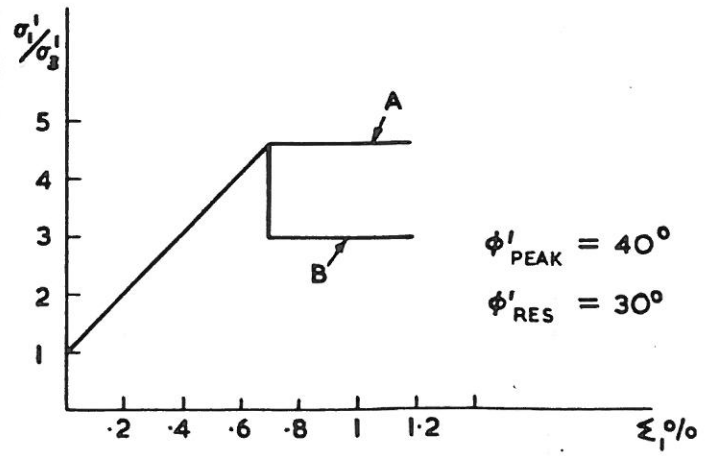

Fig.2 Frictional Stress/Strain Laws

Unfortunately, the stress/strain behaviour of frictional soil is considerably more complex than that of undrained clay. The influence of confining pressure for example, is considerable. It directly affects the shear strength of a frictional material, it has a direct influence on soil stiffness, the peak friction angle is reduced with increase in confinement with corresponding reduction in softening effects, and the volumetric dilative tendency of dense sands is suppressed. Indeed, the only parameter that is insensitive to increased confinement is the residual friction angle. Due to these difficulties in cohesionless soil behaviour, the use of complex constitutive models[3,4] seems unavoidable if the above effects are to be accounted for. Certainly, no simple shear stress/strain law as proposed for the undrained clay material would suffice.

Naturally, the complexity of any model used will depend on what a given analysis seeks to achieve. Volumetric change for example, especially in cohesionless soils, remains an extremely complex quantity to generalise for different stress paths. It is suggested however, that if collapse loads and ultimate conditions are of interest, meaningful results may be achieved, even with the greatly simplified models presented here.

STRESS/STRAIN MODELS

Cohesive Soil

The three models given in Fig.1 are all given in terms of the deviatoric stress/strain invariants $\bar{\sigma}$ and $\bar{\varepsilon}$ which were defined earlier.

Curve A is a simple elastic-perfectly plastic model fully defined by the gradient of the elastic portion which is equal to $3G$, and the peak cohesion C_{PEAK} at which plastic behaviour commences. The failure surface in this model would be a stationary cylinder in principal stress space with radius $\sqrt{2}\, C_{PEAK}$. The two parameters used in this model were as follows:

$$G = 5 \times 10^4 \text{ kN/m}^2$$
$$C_{PEAK} = 100 \text{ kN/m}^2.$$

Curve B reaches the same peak cohesion as A, but takes a more realistic path exhibiting both elastic and plastic strains given by

$$\bar{\varepsilon} = \frac{\bar{\sigma}}{3G} - A \ln \left(1 - \frac{\bar{\sigma}}{\sqrt{3}\, C_{PEAK}}\right) \qquad (9)$$

where A = constant affecting the initial gradient. Such a curve could be fitted to triaxial test results on undrained clay by adjusting G and A. The failure surface in this model is identical to A, but an infinite family of concentric yield cylinders could be visualised within it, initially of zero radius, but growing as a function of $\bar{\varepsilon}$.

The three parameters used in this model were as follows:

$$G = 3.7 \times 10^4 \text{ kN/m}^2$$
$$A = 10^{-4}$$
$$C_{PEAK} = 100 \text{ kN/m}^2.$$

Curve C requires four parameters; C_{PEAK}, C_{RES}, G and H, where H is the gradient of the softening portion. Prior to peak strength, the material behaves elastically as in model A with gradient 3G. The failure surface in this model would initially be of radius $\sqrt{2}\ C_{PEAK}$, but would shrink as a function of $\bar{\varepsilon}$ and H to a new constant radius of $\sqrt{2}\ C_{RES}$. The four parameters used in this model were as follows:

$$G = 7.41 \times 10^4\ kN/m^2$$
$$H = -5.56 \times 10^4\ kN/m^2$$
$$C_{PEAK} = 100\ kN/m^2$$
$$C_{RES} = 50\ kN/m^2.$$

The jagged shape of curve C is by no means obligatory. Any combination of mathematical functions, such as that used in B, but incorporating softening, could be used.

Frictional Soil

As stated in the Introduction, simple stress/strain behaviour is very difficult to express in a general form for this type of soil. For a given mean stress however, the simplest parameter that remains fairly constant at failure for different stress paths is the stress ratio σ_1'/σ_3' where

$$\left(\frac{\sigma_1'}{\sigma_3'}\right)_{PEAK} = \tan^2\left(45 + \frac{\phi'_{PEAK}}{2}\right) \qquad (10)$$

From the two models described in Fig.2, model A remains elastic until peak stress ratio is reached, whereupon perfectly plastic behaviour ensues. The simple softening model B, remains elastic until the peak stress ratio is reached, after which the residual surface comes into play in the form of a step reduction in strength. In a continuum analysis, all points would have a strength governed by either ϕ'_{PEAK} or ϕ'_{RES}. In principal stress space, this could be visualised as two Mohr-Coulomb hexagonal cones with the inner cone only coming into play once the outer cone had been reached.

The properties used in both models A and B involved an elastic shear modulus where

$$G = 188\ \sigma_m$$

with σ_m being the initial mean stress. The peak and residual friction angles were taken as 40^o and 30^o respectively.

Smoother transition during hardening to ϕ'_{PEAK}, and softening to ϕ'_{RES} could have been implemented if required.

The influence of mean stress on ϕ'_{PEAK} may also be incorporated and is the intended topic of a later paper. The aim of the present work however, is to fully exploit the simple models while taking account of their obvious shortcomings.

SOLUTION PROCEDURE

Plane strain finite element analyses were performed on the mesh of Fig.3.

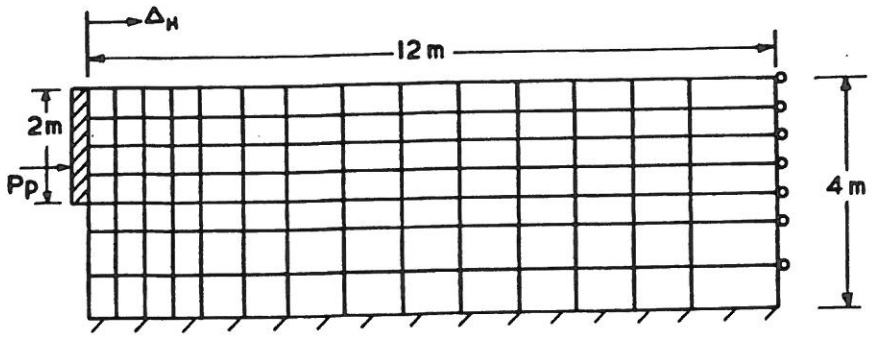

Fig.3 Mesh Used for Earth Pressures Computation

Eight-node quadrilateral elements were used with "reduced" (2 x 2) Gaussian integration in both the stiffness formulation and the plastic stress redistribution. Plasticity was introduced using the viscoplastic technique which is described elsewhere[5,6] and which has been shown[7] to be an efficient and versatile way of solving problems of elasto-plasticity.

Stresses were applied to the soil in the form of prescribed, horizontal displacements simulating an infinitely rigid wall.

The heart of the viscoplastic algorithm lies in the expression for plastic strain rate where

$$\underline{\dot{\varepsilon}}^{vp} = \gamma F \frac{\partial Q}{\partial \underline{\sigma}}^{*} . \qquad (11)$$

F represents the current yield function and may easily be made a function of any related variables. If $F = 0$, the stress state lies on the yield surface, but if $F > 0$, then yield is violated and equation 11 comes into play.

In cohesive model A, F defines a constant failure surface where

$$F_A = \bar{\sigma} - \sqrt{3}\, c_{PEAK} \qquad (12)$$

In cohesive model B, F defines a yield surface which expands as a function of $\bar{\varepsilon}$ from equation 9. At any stage of the calculation, for a given value of $\bar{\varepsilon}$, equation 9 must be solved to give the current size of the yield cylinder which is then compared with the current stress state thus

$$F_B = \bar{\sigma} - \bar{\sigma}_{eqn.9} \qquad (13)$$

In cohesive model C, F is again a function of $\bar{\varepsilon}$ and may be summarised thus:

if $\bar{\varepsilon} < \dfrac{\sqrt{3}\, c_{PEAK}}{3G}$

then

$$F_C = \bar{\sigma} - \sqrt{3}\, c_{PEAK} \qquad (14)$$

* The plastic potential Q always predicts zero plastic volume change in the present work.

else if $\frac{\sqrt{3}\, C_{PEAK}}{3G} \leqslant \bar{\varepsilon} < \frac{\sqrt{3}\, C_{PEAK}}{3G} + \frac{\sqrt{3}\, C_{RES} - \sqrt{3}\, C_{PEAK}}{H}$

then $$F_c = \bar{\sigma} - \left(\sqrt{3}\, C_{PEAK} + \left(\bar{\varepsilon} - \frac{\sqrt{3}\, C_{PEAK}}{3G}\right)H\right) \qquad (15)$$

else if $\frac{\sqrt{3}\, C_{PEAK}}{3G} + \frac{\sqrt{3}\, C_{RES} - \sqrt{3}\, C_{PEAK}}{H} \leqslant \bar{\varepsilon}$

then $$F_c = \bar{\sigma} - \sqrt{3}\, C_{RES} \qquad (16)$$

Equations 14, 15 and 16 quoted here force all Gauss points in the finite element mesh to follow curve C in Fig.1. Whereas model A required only the evaluation of $\bar{\sigma}$ for comparison with the constant failure surface, models B and C required that $\bar{\varepsilon}$ be evaluated first in order to find the current size of the yield surface before comparing stresses with it.

In models A or C, only points within the mesh in the zones of high shear stress will ever yield (Fig.5), with the great majority of the mesh remaining elastic. In model B, any amount of wall movement, no matter how small, will cause all points in the mesh to violate yield to some extent, requiring substantially more computing effort. This point may become significant in large problems where computer costs must be minimised. Generally speaking, the less Gauss points that leave the elastic zone, the cheaper the solution.

For the frictional material, model A describes a simple elasto-plastic model governed by Mohr-Coulomb's failure criterion where

$$F = \frac{\sigma_1' + \sigma_3'}{2} \sin \phi'_{PEAK} - \frac{(\sigma_1' - \sigma_3')}{2} . \qquad (17)$$

Alternatively, the material remains elastic until peak stress ratio given by equation 10 is reached, whereupon plastic yield commences.

The softening model B keeps a watch on the stress ratio at each Gauss point. Wherever it reaches the peak value, a new lower friction angle ϕ'_{RES} replaces the peak angle and the reduced strength is defined by

$$F = \frac{\sigma_1' + \sigma_3'}{2} \sin \phi'_{RES} - \frac{(\sigma_1' - \sigma_3')}{2} . \qquad (18)$$

RESULTS

Cohesive Models

The results in Fig.4 represent the build up of passive resistance (P_m) with horizontal wall strain for each of the three models. The resistance was obtained by averaging the horizontal stresses in the first column of Gauss points adjacent to the displaced nodes, and multiplying by the wall height. The ordinate plotted in Fig.4 is the 'mobilised cohesion' at each stage of the calculation where

$$C_m = \frac{P_m}{2H} . \qquad (19)$$

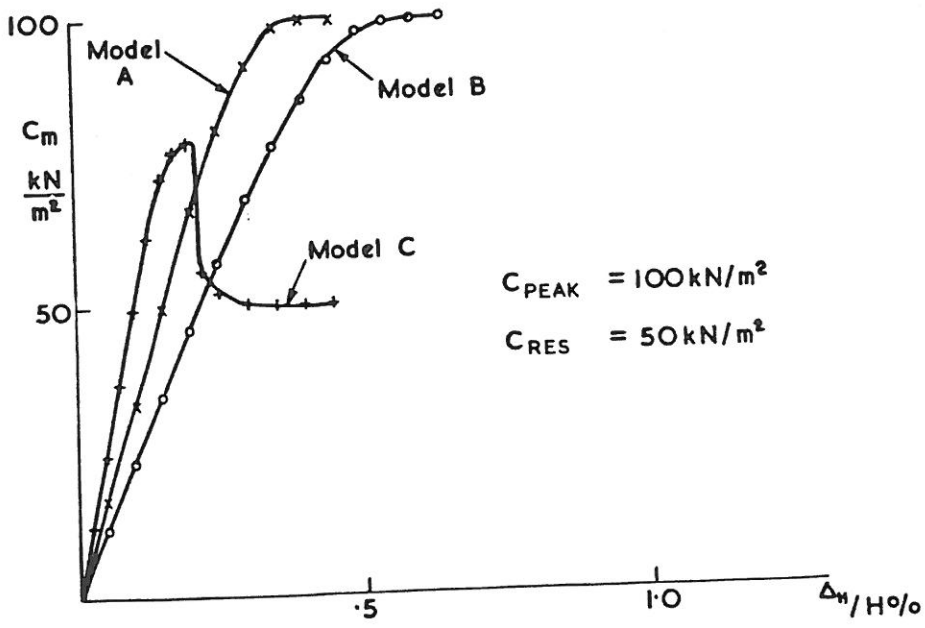

Fig.4 Build-up of Passive Resistance in Cohesive Models

Models A and B gave identical values of peak passive resistance, but model B gave a softer response due to the greater amount of plastic straining. Although model C had the same peak cohesion as A and B, the peak mobilised value in the wall problem lay between the peak and residual element values. This effect was due to progressive failure and Fig.5 shows how various parts of the yielding zone are simultaneously at different stages of softening. Only at larger values of wall strain, when a mechanism has formed comprising only of soil at its residual strength does C_m tally with C_{RES}. It is also interesting to note that in this case peak C_m (upper Fig.5) occurs before yield has spread to ground surface. The sudden reduction in C_m coincides with the formation of a plastic mechanism between the base of the wall and the ground.

Peak C_m always lies between C_{PEAK} and C_{RES}, but its position relative to these extremes depends on the brittleness properties C_{RES}/C_{PEAK} and $-H/3G$. A summary of results for different degrees of brittleness is given in Fig.6. It was found that as the steepness of the softening curve was increased, the maximum wall resistance fell due to the greater brittleness. A stage was reached however, when $-H/3G > 1$, at which increase in the softening gradient had no further effect on the wall resistance. The softening at this stage was presumably occurring so suddenly that the gradient of the transition from peak to residual was inconsequential.

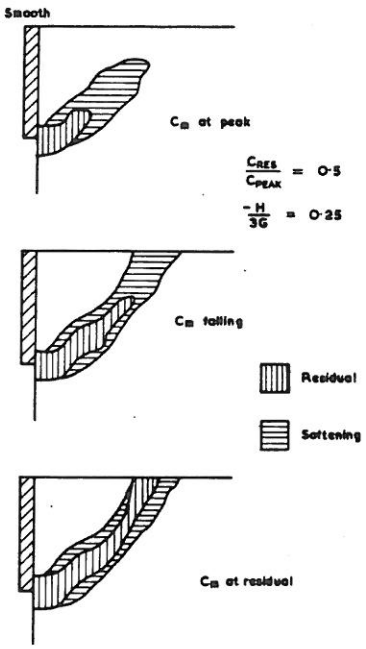

Fig.5 Spread of Yield at Different Stages of Loading in Cohesive Soil

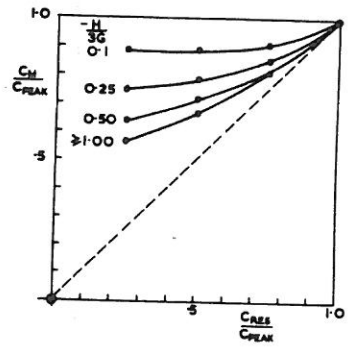

Fig.6 Effect of Strain Softening on Peak Passive Resistance

Frictional Models

The results in Fig.7 show the build-up of wall resistance for models A and B (Fig.2) in terms of a "mobilised friction angle" ϕ'_m where

$$\phi'_m = 2(\arctan \sqrt{\frac{P_m}{\frac{1}{2}\gamma H^2}} - 45^o) \qquad (20)$$

As before, the perfectly plastic material closely reproduced Rankine's solution and the softening model gave a peak ϕ'_m that lay between ϕ'_{PEAK} and ϕ'_{RES}.

In spite of the simplicity of the frictional models assumed, two important qualitative features were observed. Fig.8 reproduces the progressive failure that occurred in the soil mass. Three Gauss points were taken at varying distances from the wall. Soil near the base of the wall was seen to reach peak strength and soften while soil further away still had reserves of strength. The peak ϕ'_m in Fig.7 occurred when softening elements on the shear surface

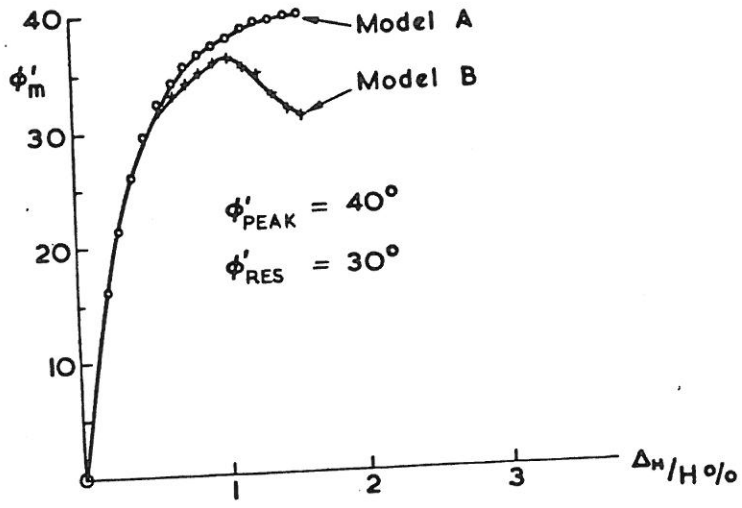

Fig.7 Build-up of Passive Resistance in Frictional Models

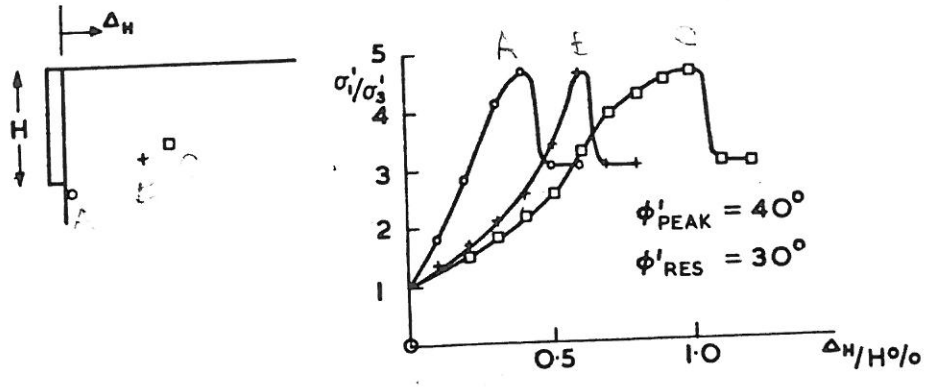

Fig.8 Progressive Failure in Softening Frictional Soil

outweighed the elements that were still hardening.

Fig.9 shows the extent of yielding in both models A and B after 1% of wall strain. The softening soil clearly yielded in a narrower zone as shear strains concentrated in the weaker soil that had reached residual conditions. This is consistent with the fact that a passive wall fails along the path of least resistance. As was observed with the cohesive soil, peak resistance was achieved before plasticity had spread to ground level.

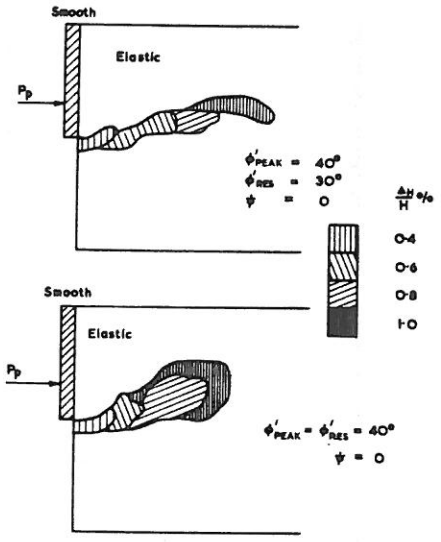

Fig.9 Effect of Softening on Spread of Yield

Continuum finite element solutions using small strain theory and crude meshes are limited in their ability to reproduce large relative movements along narrow slip surfaces. Naturally, finer meshes go some way to improving the situation, but a fair idea of the mechanisms of failure can still be obtained with crude meshes. Fig.10 shows the situation at passive failure using frictional model A. It can be seen that the great majority of movements occurred to the left of Rankine's line drawn at $45 - \phi'_{PEAK}/2$ to the horizontal.

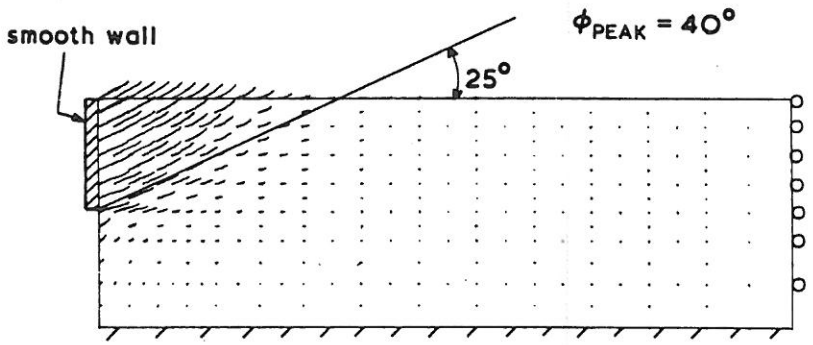

Fig.10 Nodal Displacements at Passive Failure

CONCLUDING REMARKS

The cohesive models indicated that any invariant relationship between $\bar{\sigma}$ and $\bar{\varepsilon}$ (or other compatible invariants) could form the basis of a stress/strain law for undrained clay. Strain-softening effects are easily included in these relationships which can be obtained by curve fitting laboratory triaxial data.

The form of the proposed stress/strain laws had virtually no effect on peak passive resistance provided no softening was included. When softening was incorporated, progressive failure resulted in the peak resistance lying between the peak and residual element strengths. The value of the peak resistance in this case was dependent on the shape of the stress/strain curve path pre- and post-peak and was dependent on certain dimensionless 'brittleness' parameters.

In the context of simple models, considerably less versatility is possible with frictional soils due to their added complexity. By just specifying peak and residual friction angles however, collapse loads in close agreement with Rankine could be obtained and even progressive failure with narrowing of the shearing zones detected.

Finally, reasonable mechanisms of failure could be detected from the displacement plots at failure. This was in spite of using crude meshes and simple iteration procedures.

REFERENCES

1. H.B. Poorooshasb, I. Holubec and A.N. Sherbourne, "Yielding and flow of sand in triaxial compression", Part 1, Canadian Geotech. J., v.3, No.4, 179-190 (1966)

2. P.W. Rowe and K. Peaker, "Passive earth pressure measurements", Geotechnique, 15, No.1, 57-78 (1965)

3. P.V. Lade, "Elasto - plastic stress-strain theory for cohesionless soils with curved yield surfaces", Int. J. Solids Struct., v.13, 1019-1035 (1977)

4. P.A. Vermeer, "A double hardening model for sand", Geotechnique 28, No.4, 413-433 (1978)

5. O.C. Zienkiewicz and I.C. Cormeau, "Viscoplastic solution by the finite element process", Arch. Mech., v.24, 873-888 (1972)

6. O.C. Zienkiewicz and I.C. Cormeau, "Viscoplasticity, plasticity and creep in elastic solids. A unified numerical solution approach", Int. J. Num. Meth. Eng., v.8, 821-845 (1974)

7. D.V. Griffiths, "Finite element analyses of walls, footings and slopes", Symp. Comp. Appl. to Geotech. Probs. in Highway Eng., Cambridge, U.K. (1980)

APPENDIX A

Notation

$\bar{\sigma}$, t	deviatoric invariants of stress
$d\bar{\varepsilon}$, $d\bar{\gamma}$	deviatoric invariants of strain increment
σ_x, σ_y, σ_z, τ_{xy}	Cartesian stress components
ε_x, ε_y, ε_z, γ_{xy}	Cartesian strain components
σ_m	volumetric invariant of stress
$d\bar{v}$	volumetric invariant of strain increment
dE	energy increment
G	shear modulus
C_{PEAK}	peak undrained cohesion
C_{RES}	residual undrained cohesion
A	curve fitting parameter
H	gradient of softening line, wall height
σ_1', σ_3'	principal effective stresses
ϕ'_{PEAK}	peak friction angle
ϕ'_{RES}	residual friction angle
$\underline{\varepsilon}^{vp}$	vector of viscoplastic strain rates
γ	fluidity parameter, soil unit weight
F	yield function
Q	plastic potential function
$\underline{\sigma}$	vector of stresses
C_m	mobilised cohesion in the mass
P_m	mobilised passive resistance in the mass
ϕ'_m	mobilised friction angle in the mass
ΔH	horizontal wall movement
P_p	peak passive force